AC loss characterization of striated multifilamentary YBCO coated conductors

Contract number: AOARD-04-4034

Research period: May, 2004 ~ May, 2005

Submitted on June 29, 2005

Naoyuki Amemiya

Yokohama National University

Report Documentation Page

Form Approved
OMB No. 0704-0188

1. REPORT DATE	2. REPORT TYPE	3. DATES COVERED
26 JUL 2006	**Final Report (Technical)**	**01-06-2004 to 03-06-2006**

4. TITLE AND SUBTITLE
AC loss characterization of striated multifilamentary YBCO coated conductors

5a. CONTRACT NUMBER
FA520904P0293

5b. GRANT NUMBER

5c. PROGRAM ELEMENT NUMBER

6. AUTHOR(S)
Naoyuki Amemiya

5d. PROJECT NUMBER

5e. TASK NUMBER

5f. WORK UNIT NUMBER

7. PERFORMING ORGANIZATION NAME(S) AND ADDRESS(ES)
Yokohama National University,79-5 Tokiwadai, Hodogaya,Yokohama 240-8501,NA,JAPAN

8. PERFORMING ORGANIZATION REPORT NUMBER
AOARD-044034

9. SPONSORING/MONITORING AGENCY NAME(S) AND ADDRESS(ES)
The US Resarch Labolatory, AOARD/AFOSR, Unit 45002, APO, AP, 96337-5002

10. SPONSOR/MONITOR'S ACRONYM(S)
AOARD/AFOSR

11. SPONSOR/MONITOR'S REPORT NUMBER(S)
AOARD-044034

12. DISTRIBUTION/AVAILABILITY STATEMENT
Approved for public release; distribution unlimited

13. SUPPLEMENTARY NOTES

14. ABSTRACT

The reduction of the magnetization losses by the multifilamentary structure was demonstrated successfully. The measured magnetization losses of multifilamentary YBCO-coated conductors apparently contain a hysteretic loss component in which the dissipated energy per cycle is independent of frequency and a coupling loss component in which the dissipated energy per cycle is proportional to frequency. Experimental results show that the striation for AC loss reduction is still effective even with the superconducting bridges between filaments. Using the two-dimensional FEM model for electromagnetic field analysis of coated conductors, the AC losses at various conditions were calculated numerically. The calculated losses are typical frequency-dependent AC characteristics of multifilamentary superconductors. The transverse resistances between filaments in the measured samples were determined through the comparison between the measured and calculated magnetization losses at small field amplitude. The magnetization losses calculated in a wide range of field amplitude using these transverse resistances reasonably agree with the measured magnetization losses.

15. SUBJECT TERMS
Electromagnetics, Superconductivity

16. SECURITY CLASSIFICATION OF:			17. LIMITATION OF ABSTRACT	18. NUMBER OF PAGES	19a. NAME OF RESPONSIBLE PERSON
a. REPORT	b. ABSTRACT	c. THIS PAGE			
unclassified	**unclassified**	**unclassified**		**31**	

1. Introduction

YBCO coated conductors are being considered as the next generation or second generation high temperature superconductors [1-4]. When using YBCO coated conductors for AC electrical devices, low AC loss is important. The AC loss reduction of YBCO coated conductors is particularly crucial for their application to airborne electrical devices operated at high frequencies [5]. However, the wide cross-sectional shape of the usual YBCO coated conductors is a disadvantage from the viewpoint of AC loss: when a thin strip of superconductor, such as a usual YBCO coated conductor, is exposed to the AC transverse magnetic field perpendicular to its wide face, a large magnetization loss is generated [6, 7]. One means of reducing the magnetization loss is the introduction of multifilamentary structure.

In this research project, first, the AC loss characteristics of multifilamentary YBCO coated conductors were studied experimentally. Striated multifilamentary YBCO coated conductors with 20 or 40 filaments were prepared by AFRL. Using these samples, the AC loss reduction by striation was demonstrated at high frequencies, and the detailed AC loss characteristics of multifilamentary YBCO coated conductors were studied. The influence of superconducting bridges between filaments on AC loss was also studied using another set of striated multifilamentary samples. Second, the AC loss characteristics of various multifilamentary YBCO coated conductors in a wide range of operating conditions were studied numerically. The frequency, the transverse resistance between filaments, the number (width) of filaments and the sample length were varied, and their influences on the AC loss were studied. The numerical results were compared with the experimental results.

Experiments were conducted and calculations were made for flat finite-length multifilamentary YBCO coated conductors (Fig. 1.1(a)). It should be noted that a finite-length sample with a length L simulates a half pitch of a twisted infinitely-long multifilamentary YBCO coated conductor that has a twist pitch of $2L$ (Fig. 1.1(b)) with respect to the shielding current path against the transverse magnetic field.

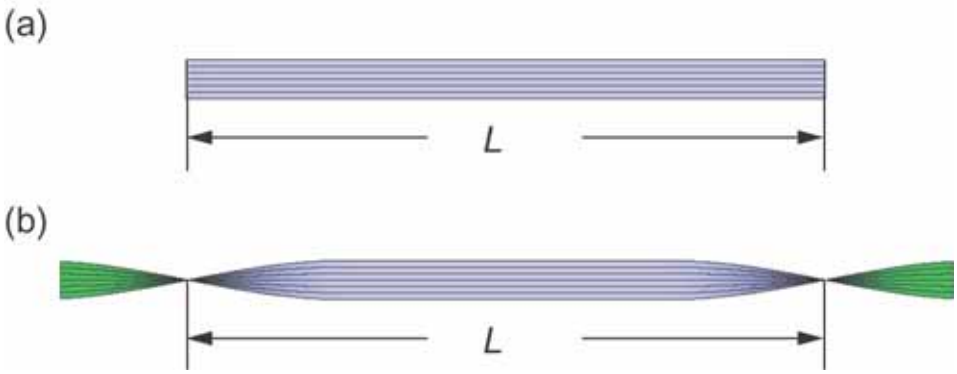

Fig. 1.1 Flat finite-length multifilamentary YBCO coated conductor (a) and half pitch of twisted infinitely-long multifilamentary YBCO coated conductor (b).

2. Experimental characterization of AC loss of striated multifilamentary YBCO coated conductors [8, 9]

2.1 Prepared samples

Specifications of the prepared samples are listed in Table 2.1. A laser ablation technique was used to striate the samples [10]. Samples ST20 and NSa were cut from a longer piece of conductor whose end-to-end critical current was 132 A. Samples ST40, NSb, ST20-WOB, ST20-MID, ST20-ALT and ST20-ZIP were cut from another longer piece of conductor whose end-to-end critical current was 173 A. The silver protective layer, YBCO layer, and buffer layer were cut through by the laser with parallel cuts. Images of the whole sample and micrograph images of filaments and grooves between filaments are shown in Fig. 2.1 (sample ST20) and in Fig. 2.2 (sample ST40).

Using a sample set consisting of samples ST20, NSa, ST40 and NSb, the effect of striation on AC loss reduction were demonstrated, and the detailed AC loss characteristics of multifilamentary YBCO coated conductors were studied. Sample ST20 was originally 100 mm long. We refer to it as ST20L. For AC loss measurements, shorter piece was cut from sample ST20L: 26.5 mm long ST20S. Sample ST40 was originally 100 mm long. We refer to it as ST40L. For AC loss measurements, shorter pieces were subsequently cut from sample ST40L: 50 mm long ST40M and 25 mm long ST40S.

Samples ST20-WOB, ST20-MID, ST20-ALT and ST20-ZIP were with different pattern of bridges between filaments. All of these samples are 100 mm long. Using this second set of samples, the influence of superconducting bridges between filaments on AC loss was studied.

2.2 Experimental method

A schematic view of the experimental setup for AC loss measurements is shown in Fig. 2.3(a) [11]. The entire system was cooled in liquid nitrogen. A sample was placed inside the bore of a dipole magnet that generated an AC transverse magnetic field. The magnetization loss was measured using a linked pick-up coil (LPC) [11]; a schematic view of the LPC is shown in Fig. 2.3(b). The height, length of one turn along the sample axis, and number of turns are denoted by h, L, and N, respectively. The magnetization loss per unit length of the sample per cycle, Q_{m}, is given as

$$Q_{\mathrm{m}} = C\frac{hH_{\mathrm{rms}}V_{\mathrm{m,in,rms}}}{NLf}, \tag{2.1}$$

where C is the calibration constant of the LPC, H_{rms} is the rms of the applied magnetic field,

$V_{m,in,rms}$ is the rms of the loss component of the output voltage of the LPC measured by a lock-in amplifier, and f is the frequency of the applied magnetic field. The cross-sectional dimension and total length of the LPC used were 33 mm × 33 mm and 48 mm, respectively. Previous research confirmed that C is not substantially influenced by either a sample width up to 10 mm or the sample orientation. The value of C can be fixed at 2.0 for this given size of the LPC when the sample is sufficiently long as compared to the total length of the LPC. In the case when the sample was shorter than the total length of the LPC, the measured loss was approximated using a correction factor based on the ratio between the total length of the LPC and the sample length. In all experiments reported here, the magnetic field is perpendicular to the wide face of conductor.

The critical current of the sample was measured by a four-probe method. The current was supplied to all filaments, and the voltage between the two voltage taps that were attached to selected filaments was measured [8]. The critical current was measured after measuring the AC loss in order to avoid any soldering influence on the AC loss measurement. Soldering of the current leads at both ends will definitely affect the measured AC loss since the solder will act as an alternate interfilamentary current path.

2.3 Experimental results and discussion

2.3.1 Effect of striation on AC loss reduction and detailed AC loss characteristics of multifilamentary YBCO coated conductors

First, the measured magnetization losses Q_m of non-striated monolithic samples NSa and NSb were plotted against the amplitude of the transverse magnetic field in Figs. 2.4(a) and 2.4(b), respectively. $Q_{c,BI}$ is the analytical value per unit length of the conductor per cycle for the non-striated monolithic conductor or completely-coupled striated multifilamentary conductor [12]:

$$Q_{c,BI} = \mu_0 w_c^{\,2} J_{cc} t H \cdot g\left(\frac{H}{H_{cc}}\right), \tag{2.2}$$

where w_c is the width of conductor, $J_{cc} = I_c/w_c t$ (t is the thickness of the YBCO layer), $H_{cc} = I_c/\pi w_c$, and $g(x)$ is the function given by equation (2.3):

$$g(x) = (2/x)\ln\cosh x - \tanh x. \tag{2.3}$$

The Q_m of sample NSa and that of sample NSb closely follow the analytical plot of $Q_{c,BI}$ in the large field region, although Q_m of sample NSa deviates from $Q_{c,BI}$ in the small field region. Such deviations have been reported previously, and one of the possible causes is a

non-uniform lateral J_c distribution [13]. It is important to note that the Q_m of these monolithic samples is almost frequency independent.

The measured magnetization losses Q_m of striated multifilamentary samples ST20 and ST40 were plotted against the amplitude of the transverse magnetic field in Figs. 2.5 and 2.6, respectively. $Q_{f,BI}$ is the analytical value per unit length of the conductor per cycle for the decoupled striated multifilamentary conductor assuming isolated filaments [12]:

$$Q_{f,BI} = \mu_0 w_f^{\,2} J_{cf} tH \cdot g\left(\frac{H}{H_{cf}}\right) n_f, \tag{2.4}$$

where w_f is the width of filament, $J_{cf} = I_c/w_f n_f t$ (n_f is the number of filaments), and $H_{cf} = I_c/\pi w_f n_f$. The Q_m of striated multifilamentary samples shown in Figs. 2.5 and 2.6 is much smaller than $Q_{c,BI,}$ except in the small field region which is of lesser interest from a practical point of view, indicating the effect of multifilamentary structure to reduce the magnetization loss. Although frequency dependent, it is rather close to $Q_{f,BI}$ in the large field region at f = 11.3 Hz. $Q_{f,BI}$ is the sum of the magnetization loss of isolated strip of superconductor--the influence of the neighboring filaments is neglected. Mawatari calculated the magnetization of an infinite array of superconducting strips based on the critical state model and pointed out that the magnetization loss of a strip is influenced by the magnetization of neighboring strips [14, 15]. Therefore, $Q_{f,BI}$ will contain an error especially when the magnetic field is small [14, 15], and this is the reason for the deviation of $Q_{f,BI}$ from Q_m in the small field region. In these figures, Q_m decreases with decreasing sample length. In shorter samples, frequency dependence in Q_m disappears.

Next, we compare the measured magnetization losses of non-striated samples and striated samples with various length more quantitatively using normalized loss plots. Here, equation (2.3) can be transformed to the following expression:

$$Q_{c,BI} = \frac{2B_m^{\,2}}{\mu_0}\frac{\pi w_c^2}{2}\left\{g\left(\frac{H}{H_{cc}}\right)\Big/\left(\frac{H}{H_{cc}}\right)\right\}, \tag{2.5}$$

where $B_m = \mu_0 H_m$. If $Q_{c,BI}$ is normalized by

$$\frac{2B_m^{\,2}}{\mu_0}\frac{\pi w_c^2}{2}, \tag{2.6}$$

and is plotted against the normalized magnetic field, H / H_{cc}, this normalized loss is independent of the critical current. This is done in Fig. 2.7(a) for the Q_m of samples NSa, ST20L, & ST20S and in Fig. 2.7(b) for the the Q_m of samples NSb, ST40L, ST40M, & ST40S as well as for $Q_{c,BI}$ and $Q_{f,BI}$, where f = 11.3 Hz, 72.4 Hz, and 171.0 Hz. For example, the

measured magnetization losses of samples ST20L and ST20S are respectively 8.9 % and 7.8 % of that of sample NSa at H / H_{cc} = 8.8 and f = 11.3 Hz.

To view the frequency-dependent loss component of the striated multifilamentary samples from another perspective, ($Q_{m,f}$-$Q_{m,11.3\ Hz}$)/(f-11.3) is plotted against $\mu_0 H_m$ in Fig. 2.8(a) for sample ST20L and in Fig. 2.8(b) for samples ST40L & ST40M, where $Q_{m,f}$ is the measured magnetization loss at f. All readings of each sample collapse to one line that is proportional to $(\mu_0 H_m)^2$: the proportionality coefficients are 1.94×10^{-8} J·m^{-1}·s·(mT)$^{-2}$·cycle^{-1} for sample ST20L, 1.56×10^{-8} J·m^{-1}·s·(mT)$^{-2}$·cycle^{-1} for sample ST40L and 3.01×10^{-9} J·m^{-1}·s·(mT)$^{-2}$·cycle^{-1} for sample ST40M, respectively, where the unit of $\mu_0 H_m$ is mT. Therefore, the $Q_{m,f}$ values of these three samples are given as

$$Q_{m,f} = 1.94 \times 10^{-8} (\mu_0 H_m)^2 (f - 11.3) + Q_{m,11.3Hz} \quad \text{for ST20L,} \tag{2.7}$$

$$Q_{m,f} = 1.56 \times 10^{-8} (\mu_0 H_m)^2 (f - 11.3) + Q_{m,11.3Hz} \quad \text{for ST40L,} \tag{2.8}$$

and

$$Q_{m,f} = 3.01 \times 10^{-9} (\mu_0 H_m)^2 (f - 11.3) + Q_{m,11.3Hz} \quad \text{for ST40M,} \tag{2.9}$$

respectively.

In the following, more detailed analysis is made for sample ST40. Using equations (2.8) and (2.9), $Q_{m,0}$, which is the hysteretic loss component, in principle, can be obtained. These extrapolated $Q_{m,0}$ values are shown in Fig. 2.9. Then, using this $Q_{m,0}$, ($Q_{m,f}$ - $Q_{m,0}$)/f/L^2 is plotted against $\mu_0 H_m$ in Fig. 2.10. All readings again roughly collapse to one line, and the proportionality coefficient is 1.4×10^{-6} J·m^{-3}·s·(mT)$^{-2}$·cycle^{-1}, where the unit of $\mu_0 H_m$ is mT. Finally, an expression to estimate the magnetization loss of ST40 for arbitrary L, f, and $\mu_0 H_m$ is obtained as

$$Q_{m,es}(L, f, \mu_0 H_m) = 1.4 \times 10^{-6} L^2 f (\mu_0 H_m)^2 + Q_{m,0}(\mu_0 H_m), \tag{2.10}$$

where the transverse resistance between filaments is unknown but is assumed to be constant. $Q_{m,0}(\mu_0 H_m)$ is given as Fig. 2.9, but in a high field region, we can roughly but conveniently substitute $Q_{f,BI}$ instead, whose analytical expression is provided [8, 12]. Generally, the coupling loss per cycle is proportional to f when f is below $1/2\pi\tau_c$, where τ_c is the coupling time constant.

If the field amplitude is reduced, we can widely vary the frequency with a given output voltage of the power supply and a given impedance of the magnet generating the applied magnetic field. In Fig. 2.11(a), Q_m of samples ST40L, ST40M, and ST40S are plotted against frequency up to 1 kHz, where $\mu_0 H_m$ = 0.5 mT or 1.0 mT. In Fig. 2.11(a), Q_m is apparently

proportional to frequency in the high frequency region. With decreasing frequency, a loss component that is independent of frequency appears. It is most remarkable in ST40S. This frequency-independent component should be the hysteretic loss in each filament. With increasing frequency or with increasing sample length, a coupling loss component becomes dominant, and then, the loss becomes proportional to frequency. Fig. 2.11(b) shows a plot of Q_m divided by $L^2(\mu_0 H_m)^2$. In a high frequency region where the coupling loss component is dominant, all readings roughly collapse to one line and are proportional to frequency f. The measured loss is dominated by the coupling loss component that is proportional to $L^2(\mu_0 H_m)^2 f$.

We define the loss reduction ratio β as follows:

$$\beta = \alpha Q_{st} / Q_{ns} , \tag{2.11}$$

where Q_{st} and Q_{ns} are the magnetization losses of striated multifilamentary and reference non-striated monolithic YBCO coated conductors, respectively, and α is a correction factor for reduction of critical current due to striation which is given as

$$\alpha = I_{c,ns} / I_{c,st} . \tag{2.12}$$

Here, $I_{c,ns}$ and $I_{c,st}$ are the critical currents of the reference non-striated monolithic and striated multifilamentary YBCO coated conductors, respectively. The experimentally observed value for β is $\alpha Q_m/Q_{c,n}$, whereas the theoretically expected value in the case of complete decoupling is given as $\alpha Q_{f,n}/Q_{c,n}$. Here, $Q_{c,n}$ and $Q_{f,n}$ are the magnetization losses of the monolithic and completely-decoupled multifilamentary YBCO coated conductors calculated by the one-dimensional FEM model (see **3.1**) using the particular values of $I_{c,ns}$ and $I_{c,st}$. These experimental and theoretical values are plotted against $\mu_0 H_m$ in Fig. 2.12, where $I_{c,st}$ is 100 A and three values of $I_{c,ns}$ are assumed: 100 A which equals $I_{c,st}$, 125 A based on an identical critical current density in the multifilamentary and monolithic conductors, and 173 A which is the original end-to-end critical current. In sample ST40M, the measured β is less than 5% at a high field region even at 72.4 Hz, whereas the theoretical β for a completely decoupled state is approximately 2%.

2.3.2 Influence of superconducting bridges between filaments on AC loss

In Fig. 2.13, the measured magnetization losses Q_m of samples ST20-WOB, ST20-MID, ST20-ALT and ST20-ZIP were plotted against the field amplitude. No major difference can be seen between the AC loss characteristics of these samples without and with various types of bridges. The striation for AC loss reduction is still effective even with the superconducting bridges between filaments. The detailed data analysis was made by AFRL.

Table 2.1 Specifications of measured samples.

	ST20 (AFRL200310B)	NSa (AFRL200310A)	ST40 (AFRL2004A2)	NSb (AFRL2004A0)
Width of conductor	10 mm	10 mm	10 mm	10 mm
Number of filaments	20	(monofilament)	40	(monofilament)
Width of filament	400 μm	N/A	200 μm	N/A
Width of groove between filaments	100 μm	N/A	50 μm	N/A
Thickness of YBCO layer	1.4 μm	1.4 μm	1.4 μm	1.4 μm
Thickness of silver protective layer	5.1 μm	5.1 μm	5.1 μm	5.1 μm
Critical current	110 A	184 ± 3 A	100 A	164 A

	ST20-WOB (AFRL2004A1)	ST20-MID (AFRL2004A3)	ST20-ALT (AFRL2004A4)	ST20-ZIP (AFRL2004A5)
Width of conductor	10 mm	10 mm	10 mm	10 mm
Number of filaments	20	20	20	20
Bridges between filaments	None	One 200 μm bridges in the middle	Two alternating 200 μm bridges per groove	Zipper pattern bridges
Width of filament	400 μm	400 μm	400 μm	400 μm
Width of groove between filaments	100 μm	N/A	50 μm	N/A
Thickness of YBCO layer	1.4 μm	1.4 μm	1.4 μm	1.4 μm
Thickness of silver protective layer	5.1 μm	5.1 μm	5.1 μm	5.1 μm
Critical current	(173 A)#	(173 A)#	(173 A)#	(173 A)#

* Substrate of all samples is Hastelloy, and their buffer layer is non-conducting.
# End-to-end critical current of original longer conductor before striation.

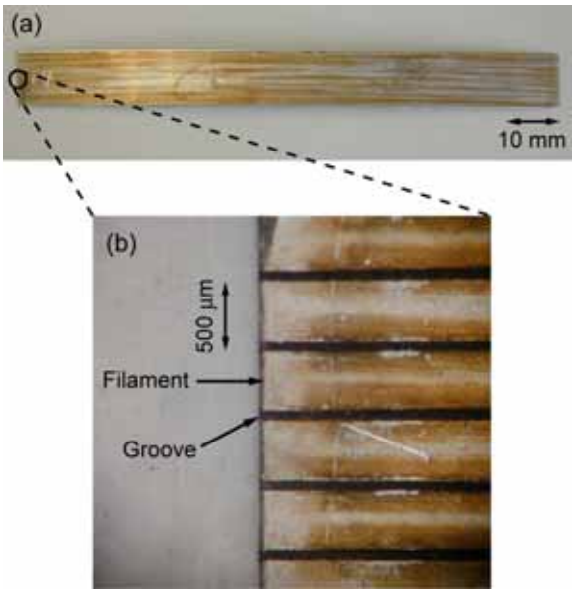

Fig. 2.1 Images of sample ST20.

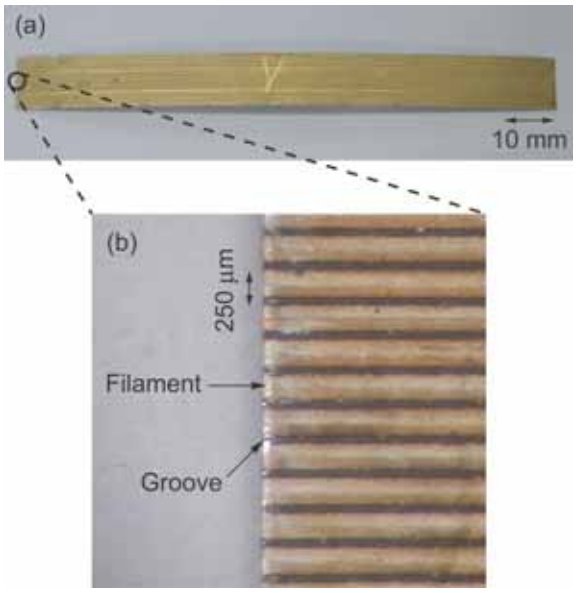

Fig. 2.2 Images of sample ST40.

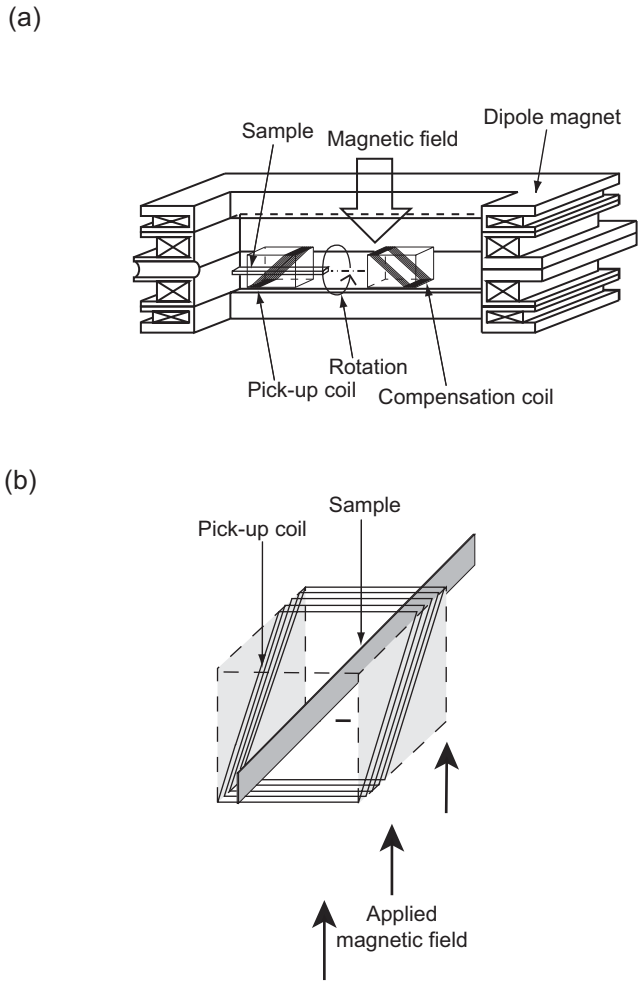

Fig. 2.3 Experimental setup: a schematic view of the entire setup (a) and the linked pick-up coil (LPC) (b).

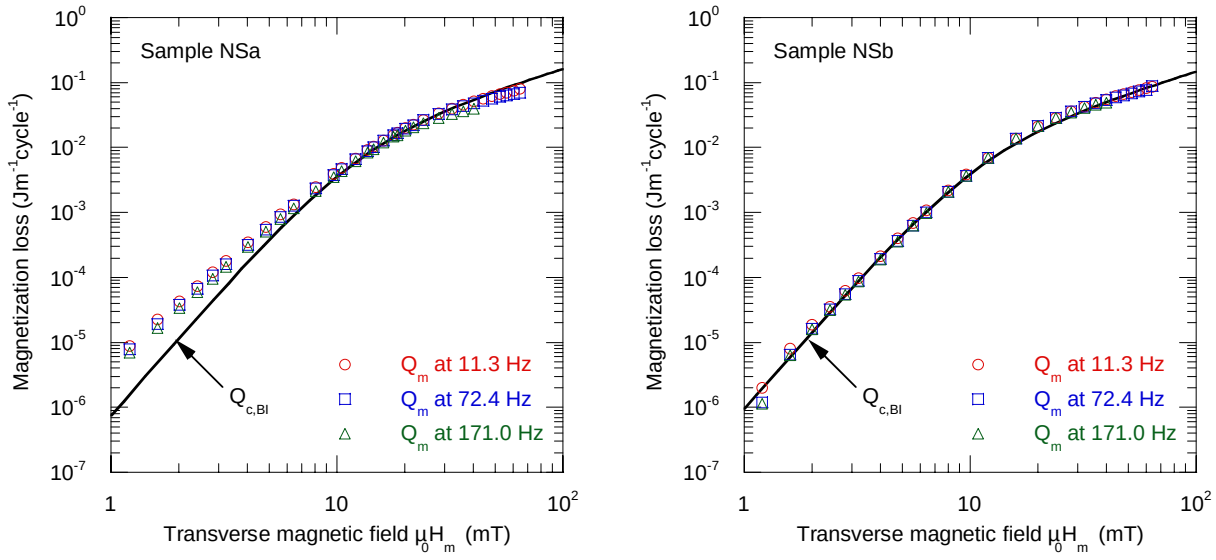

(a) Sample NSa (b) Sample NSb

Fig. 2.4 Magnetization losses of non-striated monolithic samples.

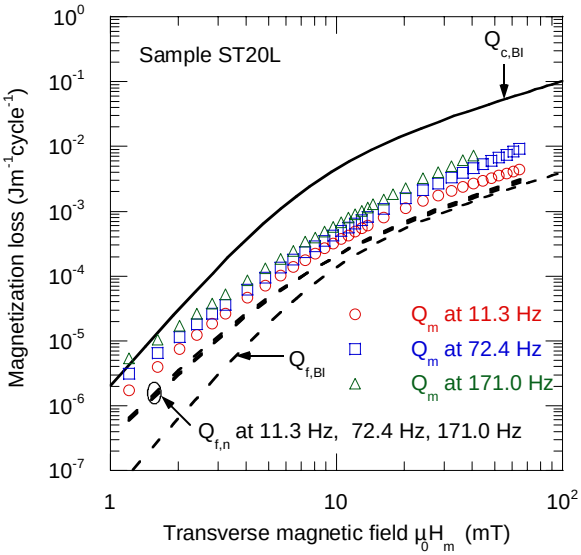

(a) 100 mm-long sample ST20L

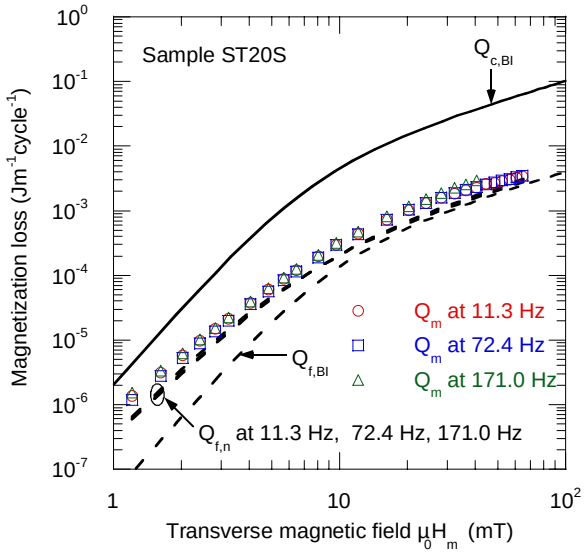

(b) 26.5 mm-long sample ST20S

Fig. 2.5 Magnetization losses of striated multifilamentary sample ST20.

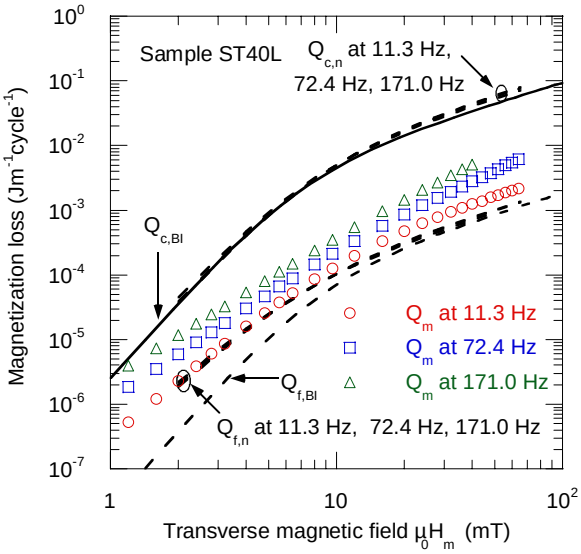

(a) 100 mm-long sample ST40L

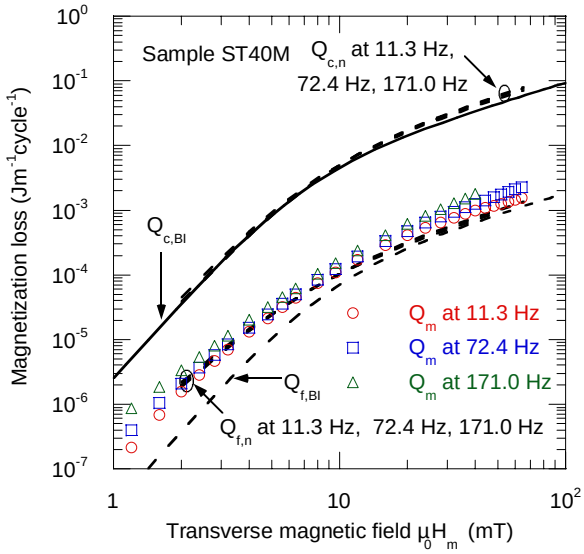

(b) 50 mm-long sample ST40M

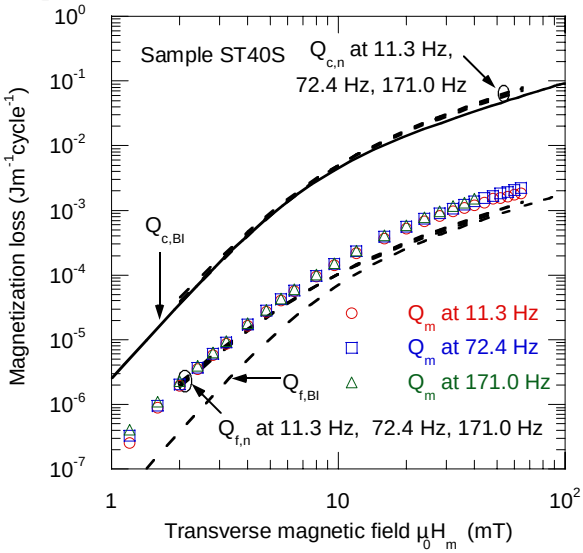

(c) 25 mm-long sample ST40S

Fig. 2.6 Magnetization losses of striated multifilamentary sample ST40.

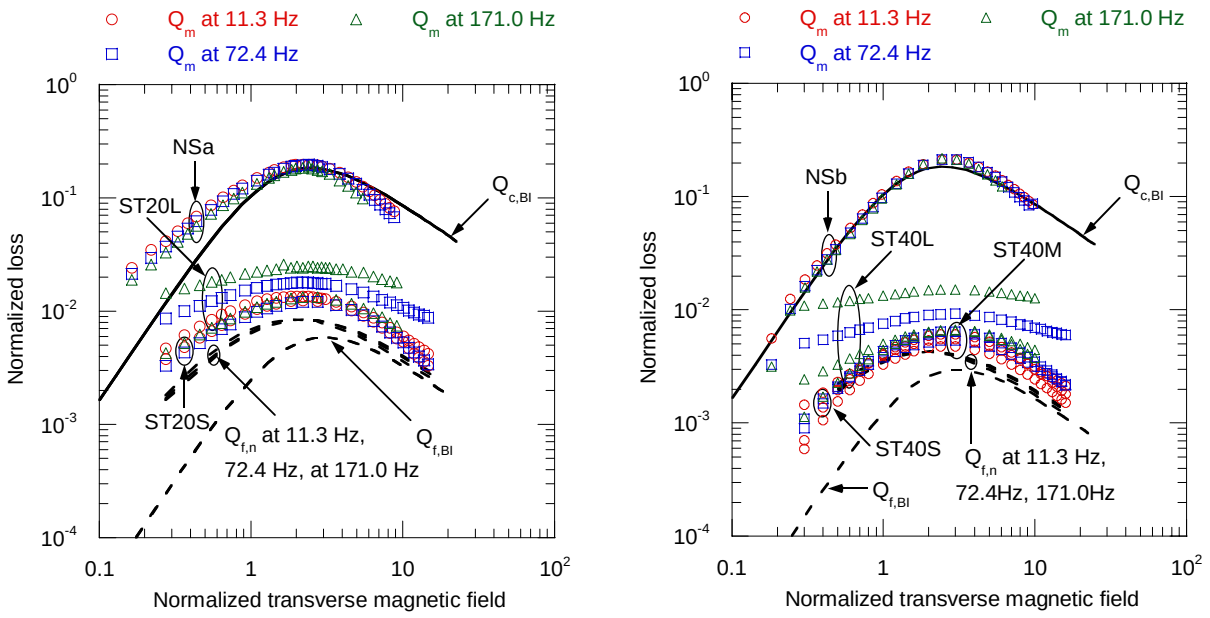

(a) NSa and ST20 (b) NSb and ST40

Fig. 2.7 Normalized losses of non-striated monolithic samples and striated multifilamentary samples.

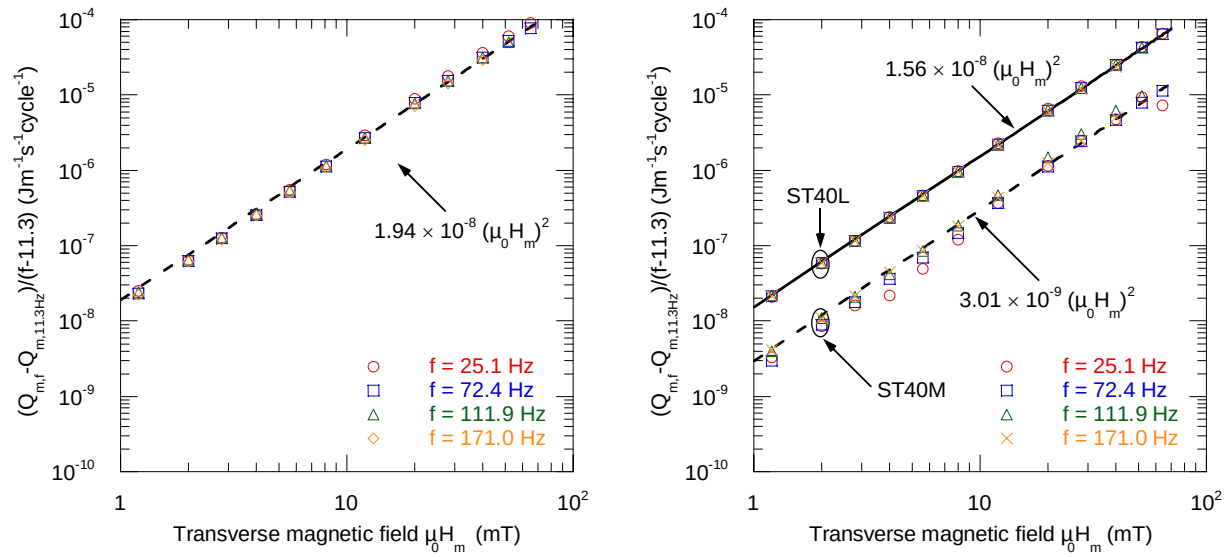

(a) ST20 (b) ST40

Fig. 2.8 $(Q_{m,f}\text{-}Q_{m,11.3\ Hz})/(f\text{-}11.3)$ of striated multifilamentary samples ST20 and ST40.

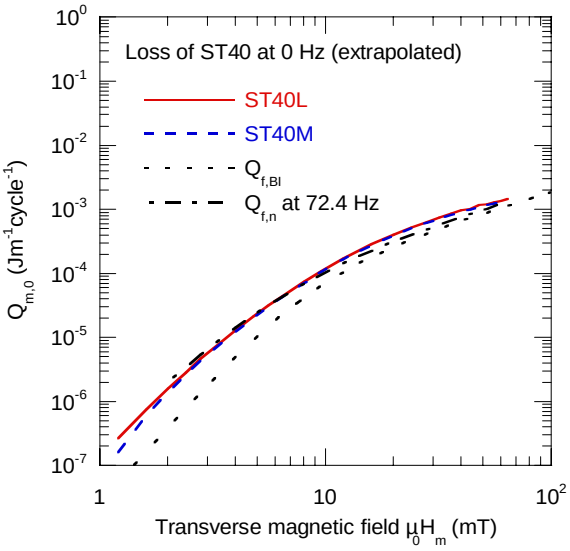

Fig. 2.9 Extrapolated hysteretic loss component of striated multifilamentary sample ST40.

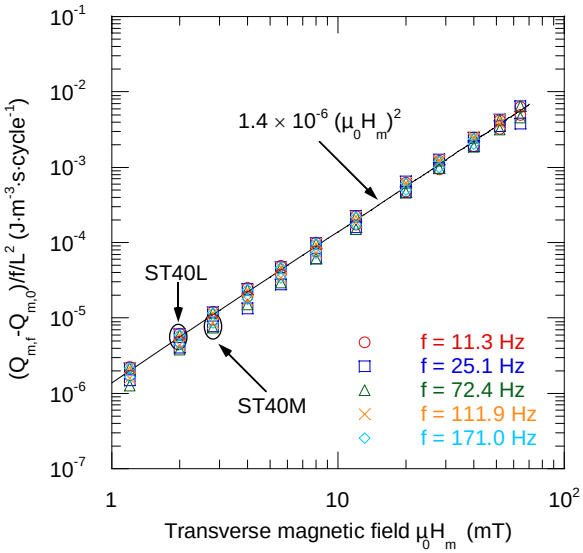

Fig. 2.10 Coupling loss component divided by fL^2, $(Q_{m,f} - Q_{m,0})/f/L^2$, of striated multifilamentary sample ST40.

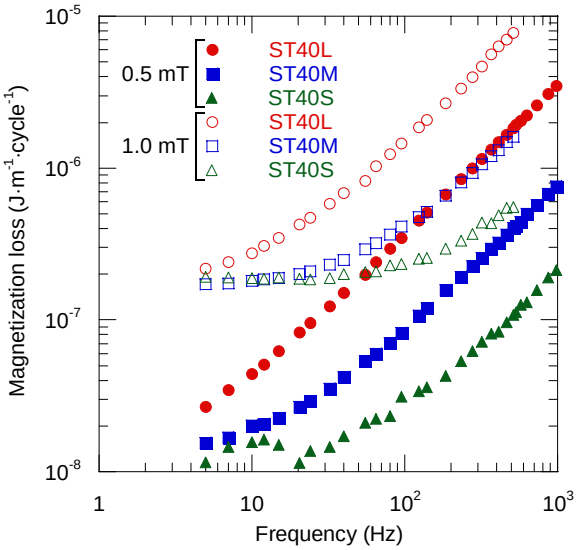

(a) Magnetization loss Q_m

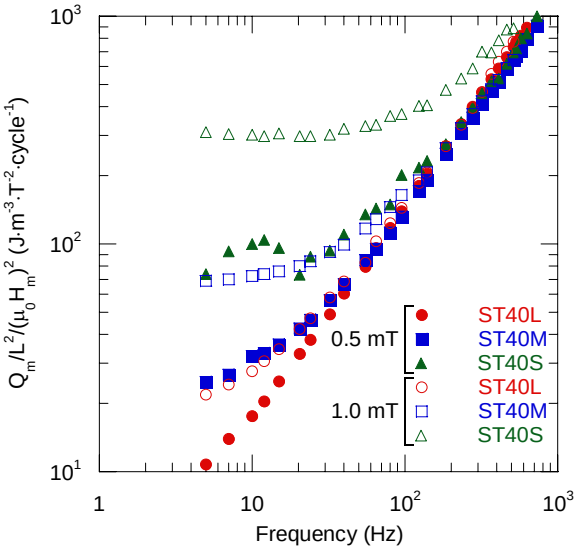

(b) Q_m divided by $L^2(\mu_0 H_m)^2$

Fig. 2.11 Magnetization loss Q_m and Q_m divided by $L^2(\mu_0 H_m)^2$ of striated multifilamentary sample ST40 at small field amplitudes.

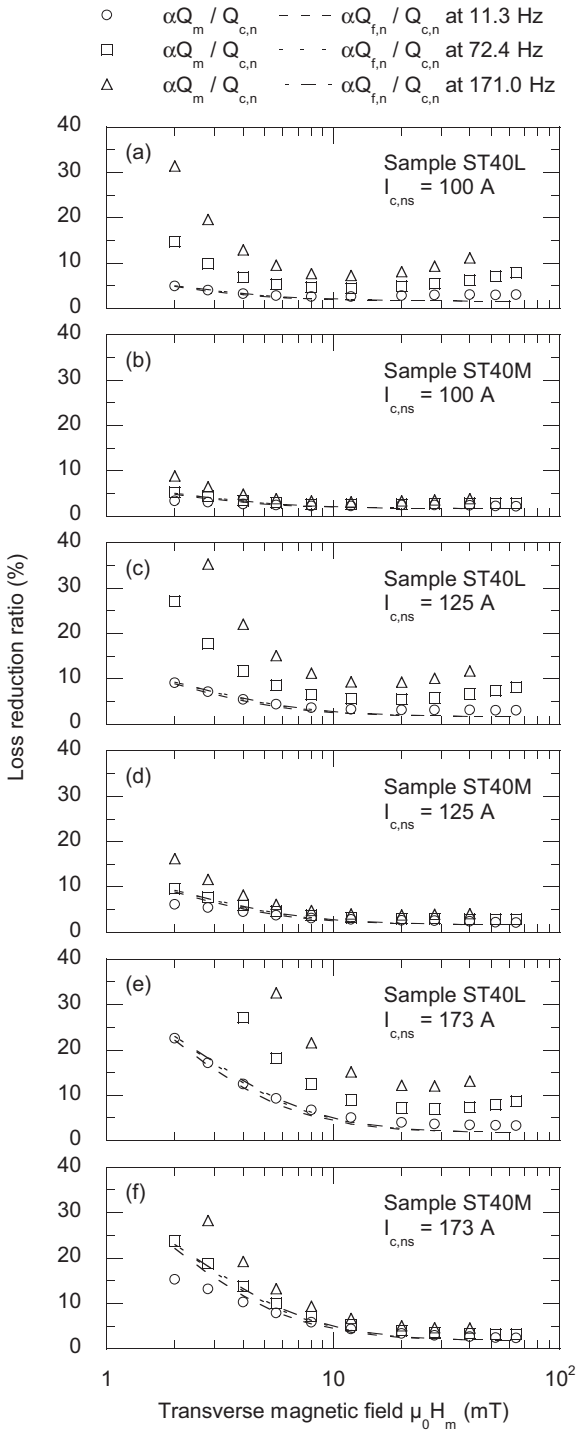

Fig. 2.12 Loss reduction ratio versus $\mu_0 H_m$.

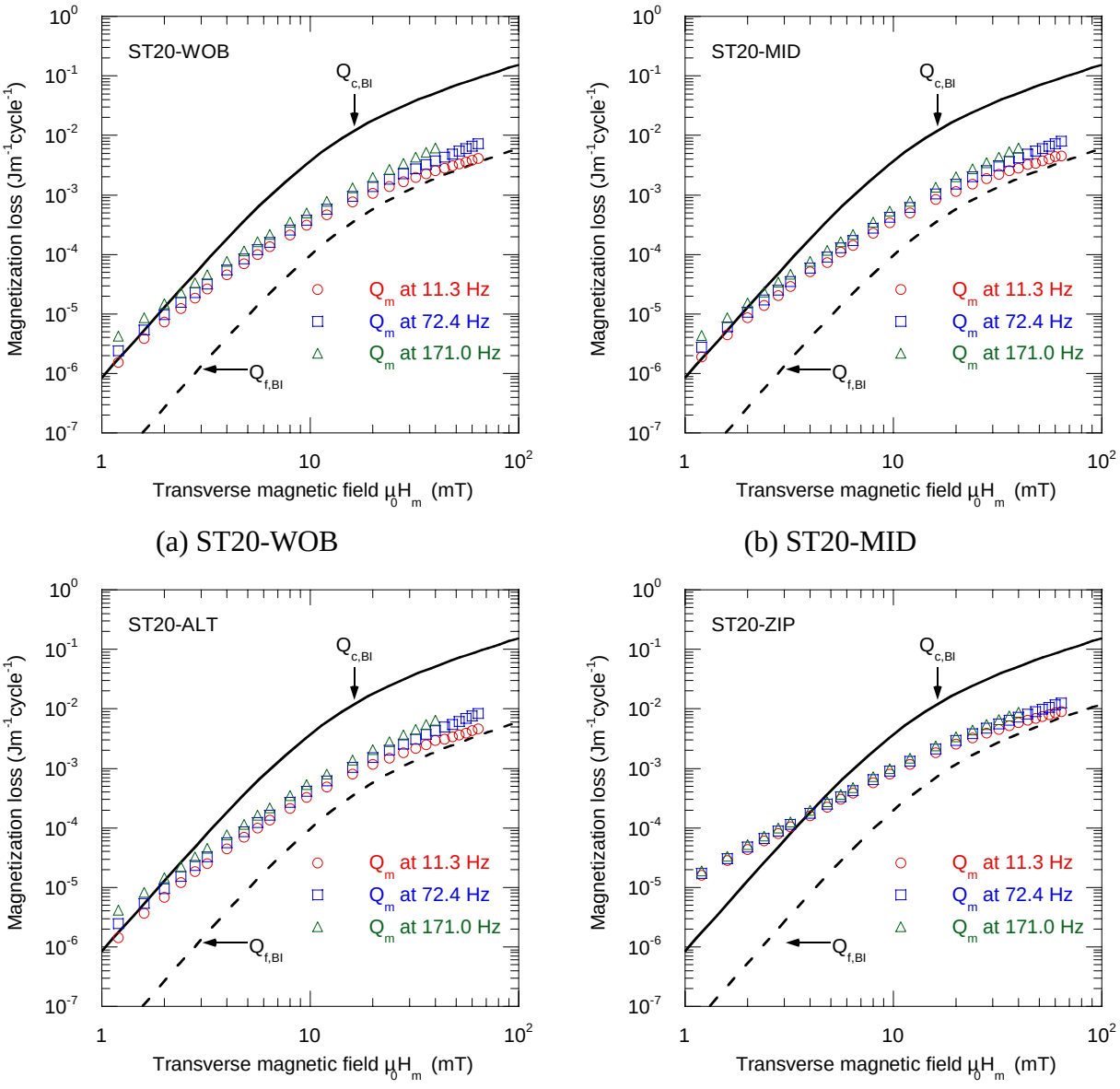

(a) ST20-WOB (b) ST20-MID

(c) ST20-ALT (d) ST20-ZIP

Fig. 2.13 Measured magnetization losses of striated multifilamentary samples with superconducting bridges between filaments.

3. Numerical characterization of AC loss of multifilamentary YBCO coated conductors [9, 16]

3.1 Numerical method

Two numerical models were used in the analysis: one-dimensional FEM model to calculate the current distribution across an YBCO coated conductor [8, 17] and two-dimensional FEM model to calculate the current distribution in the wide face of a finite-length multifilamentary YBCO coated conductor [18]. Using the one-dimensional model, the magnetization loss of monolithic conductor and completely decoupled multifilamentary conductor can be calculated. Using the two-dimensional model, the magnetization loss of multifilamentary conductor at partially decoupled state can be calculated: frequency-dependent AC loss characteristics of multifilamentary conductor can be studied. In both models, the superconducting property was given by a power law *E-J* characteristic [19],

$$E = E_0 \left(\frac{J}{J_c} \right)^n , \tag{3.1}$$

where $E_0 = 1 \times 10^{-4}$ V/m. The equivalent resistivity of superconductor was derived as

$$\rho_{sc} = \frac{E}{J} = \frac{E_0}{J_c} \left(\frac{J}{J_c} \right)^{n-1} . \tag{3.2}$$

Ohm's law with this equivalent resistivity was used as the constitutive equation to solve Maxwell's equations. The current vector potential $\boldsymbol{T}$ defined as

$$\boldsymbol{J} = \nabla \times \boldsymbol{T}, \tag{3.3}$$

was used instead of the current density $\boldsymbol{J}$ for the formulation. The current density component normal to the conductor was neglected, and only the magnetic field component normal to the conductor was considered. Thus, $\boldsymbol{T}$ had a component normal to the conductor alone.

In the one-dimensional FEM model, the governing equation derived from Maxwell's equations was

$$-\frac{\partial}{\partial y} \rho \frac{\partial T}{\partial y} = -\frac{\partial}{\partial t} \left(\frac{\mu_0 t_s}{2\pi} \int \frac{1}{y - y'} \cdot \frac{\partial T}{\partial y} \mathrm{d}y' \right) - \frac{\partial B_0}{\partial t}, \tag{3.4}$$

where y is the coordinate in the lateral direction of the conductor, ρ is the resistivity which is equal to ρ_{sc} given by equation (3.2) in superconductor, t_s is the thickness of the YBCO layer, and B_0 is the externally applied magnetic field component normal to the conductor. The first

term on the right side of equation (3.4) was the contribution of the self magnetic field. The cross-sectional models of the conductor for the analysis are shown in Fig. 3.1.

In the two-dimensional FEM model, the governing equation derived from Maxwell's equations was

$$\nabla\times(\rho\nabla\times\boldsymbol{n}T)\cdot\boldsymbol{n}=-\frac{\mu_0 t_s}{4\pi}\frac{\partial}{\partial t}\iint_S\frac{\{\nabla\times(\boldsymbol{n}T)\}\times\boldsymbol{r}\cdot\boldsymbol{n}}{r^3}\mathrm{d}S-\frac{\partial\boldsymbol{B}_0}{\partial t}\cdot\boldsymbol{n}, \tag{3.5}$$

where $\boldsymbol{r}$ is the vector from the source point to the field point, and $\boldsymbol{n}$ is the normal vector to the wide face of the conductor. The two-dimensional region for analysis in the wide face of a finite-length YBCO coated conductor is shown in Fig. 3.2. In superconductor, ρ is ρ_{sc} given by equation (3.2), and, in grooves between filaments, ρ is set at a constant value ρ_{nc} assumed as

$$\rho_{nc}=R_g\frac{t_s}{w_g}, \tag{3.6}$$

where R_g is the transverse resistance between two filaments for meter (see Fig. 3.3).

In each model, a system of nonlinear equations was obtained by discretizing equations (3.4) or (3.5) spatially by the finite element method and was solved iteratively using a relaxation method.

3.2 Numerical results and discussion

3.2.1 AC loss characteristics of various multifilamentary YBCO coated conductors in a wide range of operating conditions

The specifications of multifilamentary and monolithic conductors for calculations are listed in Table 3.1. The specifications were varied widely to clarify the potential of multifilamentary YBCO coated conductors. In the following, the calculated results using the two-dimensional model are given, unless it is mentioned that the results were calculated by the one-dimensional model. Except the analysis whose results are shown in Figs. 3.9, 3.14 and 3.15(b), L was fixed at 100 mm. Except the analysis whose results are shown in Figs. 3.10 and 3.11, w_c was fixed at 10 mm.

Fig. 3.4 shows magnetic flux contours of a multifilamentary YBCO coated conductor exposed to a transverse magnetic field at f = 10 Hz, 1 kHz, and 100 kHz, where $\mu_0 H_m$ = 50 mT, ωt = 90 degrees, L = 100 mm, R_g = 1 μΩ, n_f = 20, w_f = 400 μm and w_g = 100 μm. Half of 100 mm-long conductor is shown in this figure; right side in the figures is conductor center. Lateral cuts of Figs. 3.4(a) and 3.4(c) are shown in Fig. 3.5(a): the distributions of magnetic flux density across the center of the multifilamentary YBCO coated conductor with R_g = 1 μΩ

at f = 10 Hz and 100 kHz. Fig. 3.5(b) is the distributions of magnetic flux density of another conductor with R_g = 100 μΩ at f = 10 Hz and 1 MHz. In these figures, the filaments are decoupled completely and the shielding current flows inside each filament when the frequency is 10 Hz for both conductors with R_g = 1 μΩ and 100 μΩ; on the other hand, the filaments are coupled and the shielding current flows across the transverse resistance between filaments at 100 kHz for the conductor with R_g = 1 μΩ and at 1 MHz for the conductor with R_g = 100 μΩ, respectively.

This change in the magnetic flux distribution results in frequency-dependent magnetization loss characteristics: the magnetization losses and loss components are plotted against frequency in Figs. 3.6(a) and 3.7(a) for R_g = 1 μΩ and 100 μΩ, respectively, where amplitude of the magnetic field $\mu_0 H_m$ is 50 mT. Here, Q_{sc} is hysteretic loss in superconducting material, Q_{cp} is coupling loss, Q_{mg} is total magnetization loss of YBCO coated conductor, and $Q_{f,1\text{-}D}$ is the magnetization loss at a completely decoupled state calculated using the one-dimensional model; $Q_{c,2\text{-}D}$ is the magnetization loss of the reference monolithic conductor. In Fig. 3.6(a) where R_g = 1 μΩ, Q_{cp} is proportional to frequencies below 500 Hz, while above 500 Hz, it decreases with decreasing frequency. Q_{sc} and Q_{mg} approach $Q_{f,1\text{-}D}$ with decreasing frequency and approach $Q_{c,2\text{-}D}$ with increasing frequency. The characteristic frequency where Q_{cp} reaches its maximum increases with increasing R_g: it is around 10^5 Hz when R_g = 100 μΩ as shown in Fig. 3.7(a). In Figs. 3.6(b) and 3.7(b), Q_{mg} are plotted against $\mu_0 H_m$ at various frequencies where R_g = 1 μΩ and 100 μΩ, respectively: Q_{mg} increases with increasing frequency, and this increase is more remarkable at higher field amplitude. When R_g = 100 μΩ, Q_{mg} at f = 50 Hz calculated by the two-dimensional model closely follows $Q_{f,1\text{-}D}$ which gives the loss at a completely decoupled state; at $\mu_0 H_m$ = 0.5 T and f = 500 Hz, for example, Q_{mg} is substantially larger than $Q_{f,1\text{-}D}$. More increase in R_g is required for AC loss reduction at higher frequency and higher magnetic field.

The influence of the R_g on AC loss characteristics was studied in detail. Fig. 3.8(a) shows the frequency dependence of Q_{cp}, where $\mu_0 H_m$ is fixed at 50 mT, and R_g is 1 mΩ – 1 μΩ. Q_{cp} is inversely proportional to R_g below a characteristic frequency yielding the maximum in Q_{cp}-f curve. The characteristic frequency increases with increasing frequency. In Fig. 3.8(b), Q_{mg} is plotted against $\mu_0 H_m$ at various values of R_g when f = 50 Hz.

In Fig. 3.9, $Q_{cp}/(fL^2/R_g)$ is plotted against $\mu_0 H_m$ for various conditions listed in Table 3.2. All data fit very well to one line, which is proportional to $(\mu_0 H_m)^2$, and the proportionality coefficient is 7.8×10^{-12} J·m^{-3}·s·Ω·(mT)$^{-2}$·cycle^{-1}, where the unit of $\mu_0 H_m$ is mT. Then, an

expression to estimate the coupling loss for arbitrary L, R_g, f, and $\mu_0 H_m$ is obtained as

$$Q_{cp}(L, R_g, f, \mu_0 H_m) = 7.8\times10^{-12}(L^2 / R_g) f (\mu_0 H_m)^2. \quad (3.7)$$

In low-frequency region where filaments are almost decoupled, the magnetization loss can be estimated by the sum of Q_{cp} given by equation (3.7) and $Q_{f,BI}$ in a region of relatively high magnetic field, because the error in $Q_{f,BI}$ is not very large when $\mu_0 H_m$ is large. This is interesting from a practical point of view.

The influence of number of filaments and width of conductors is shown in Figs. 3.10 and 3.11 for R_g = 1 μΩ and 100 μΩ, respectively; the conductors with 20, 10, or 5 filaments are 10 mm wide, and the conductor with 8 filaments is 4 mm wide. Q_{mg} at $\mu_0 H_m$ = 50 mT is plotted against f in Figs. 3.10(a) and 3.11(a); Q_{sc} and Q_{cp} at $\mu_0 H_m$ = 50 mT are plotted against f in Figs. 3.10(b) and 3.11(b); Q_{mg} at $\mu_0 H_m$ = 0.5 T is plotted against f in Figs. 3.10(c) and 3.11(c); Q_{sc} and Q_{cp} at $\mu_0 H_m$ = 0.5 T are plotted against f in Figs. 3.10(d) and 3.11(d); Q_{mg} at f = 50 Hz is plotted against $\mu_0 H_m$ in Figs. 3.10(e) and 3.11(e). The values of Q_{cp} in all the conductors are almost equal when the filaments are decoupled: Q_{cp} is almost independent of the number and width of filaments. Q_{sc} is proportional to the filament width when the filaments are decoupled and is proportional to the conductor width when the filaments are coupled.

3.2.2 Comparison between measured and calculated magnetization losses

The measured and calculated magnetization losses were compared with each other for samples ST20 and ST40. In Figs. 3.12 and 3.14, measured $Q_m/L^2/(\mu_0 H_m)^2$ is plotted against frequency for samples ST20 and ST40, respectively. In these figures, $Q_m/L^2/(\mu_0 H_m)^2$ is apparently proportional to frequency in the high frequency region. The transverse resistance between filaments R_g was estimated by the comparison between the measured loss and the loss calculated by the two-dimensional FEM model where L = 100 mm: ρ_{nc} (R_g) was varied in the calculation to fit the calculated losses to the measured losses in Figs. 3.12 and 3.14. The calculated losses best fit to the measured loss when R_g = 4 μΩ for sample ST20 and R_g = 3 μΩ for sample ST40, respectively. Next, the field amplitude was varied widely, and the magnetization losses of samples ST20L and ST40L were calculated for f = 11.3 Hz, 72.4 Hz & 171.0 Hz, using the two-dimensional FEM model where R_g were set at the above fitted values. The calculated hysteretic losses in the low field region contain large numerical error, because the number of elements across each filament is limited. Therefore, the calculated losses of samples ST20L and ST40L are plotted against $\mu_0 H_m$ over 20 mT in Figs. 3.13(a) and

3.15(a), respectively. The calculated magnetization losses reasonably agree with the measured magnetization losses. The coupling losses contain less error even in the low field region, because their accuracy does not depend on the number of element across each filament. In Figs. 3.13(b) and 3.15(b), the measured and calculated $(Q_{m,f} - Q_{m,0})/f/L^2$ are plotted against $\mu_0 H_m$ for samples ST20 and ST40, respectively. It is to be noted that L was set at 100 mm and 50 mm in the calculations for Fig. 3.15(b). The measured values of $(Q_{m,f} - Q_{m,0})/f/L^2$ agree well with the calculated plots indicating that measured "$Q_{m,f} - Q_{m,0}$" is indeed the coupling loss component.

Table 3.1 Specifications of multifilamentary and monolithic conductors for calculations.

	Multifilamentary	Monolithic
Length of conductor L (m)	$2.5 \times 10^{-2} – 1.0 \times 10^{-1}$	1.0×10^{-1}
Width of conductor w_c (m)	$4.0 \times 10^{-3} – 1.0 \times 10^{-2}$	1.0×10^{-2}
Thickness of YBCO layer t_s (m)	1.0×10^{-6}	1.0×10^{-6}
Critical current density J_c (A)	2.0×10^{10}	1.6×10^{10}
n value	20	20
Width of filament w_f (m)	$4.0 \times 10^{-4} – 1.6 \times 10^{-3}$	N/A
Width of groove between filaments w_g (m)	$1.0 \times 10^{-4} – 4.0 \times 10^{-4}$	N/A
Number of filaments n_f	5 – 20	N/A
Transverse resistance between filaments per meter R_g (Ω)	$1.0 \times 10^{-3} – 1.0 \times 10^{-6}$	N/A

* The ratio of the width of filament with the width of groove is identical in all conductors.

Table 3.2 List of various conditions for analysis for scaling of coupling loss.

ID	Frequency f	Length of conductor L	Transverse resistance between filaments per meter R_g
1	50 Hz	100 mm	1.0×10^{-4} Ω
2	100 Hz	100 mm	1.0×10^{-4} Ω
3	1000 Hz	100 mm	1.0×10^{-4} Ω
4	50 Hz	100 mm	1.0×10^{-3} Ω
5	50 Hz	100 mm	1.0×10^{-5} Ω
6	50 Hz	50 mm	1.0×10^{-4} Ω
7	50 Hz	25 mm	1.0×10^{-4} Ω
8	100 Hz	50 mm	1.0×10^{-6} Ω
9	100 Hz	25 mm	1.0×10^{-6} Ω

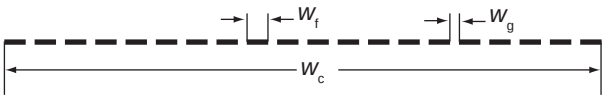

Fig. 3.1 Conductor cross-sectional view for one-dimensional FEM model.

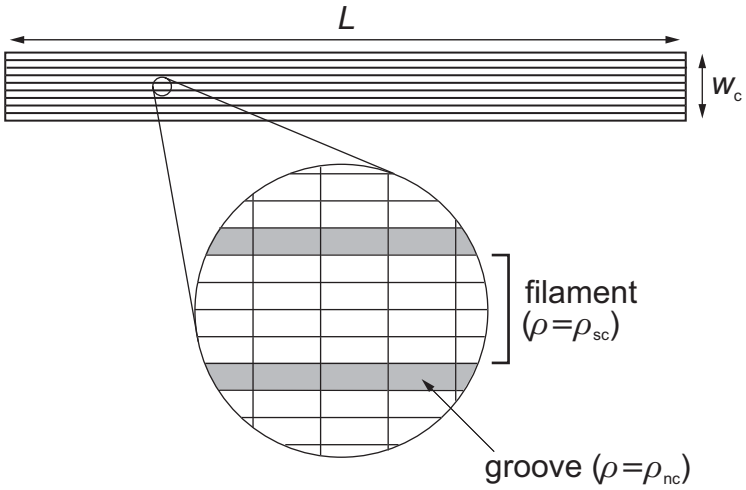

Fig. 3.2 Conductor top view for two-dimensional FEM model.

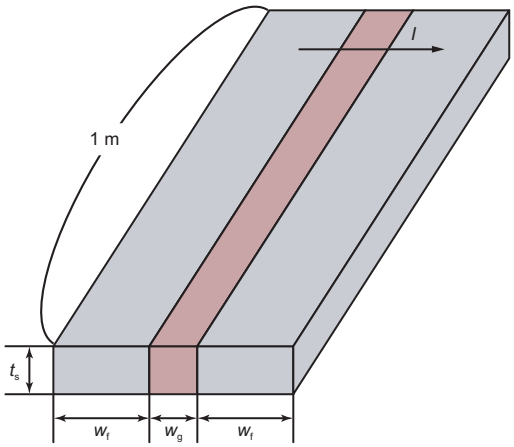

Fig. 3.3 Transverse resistance between filaments.

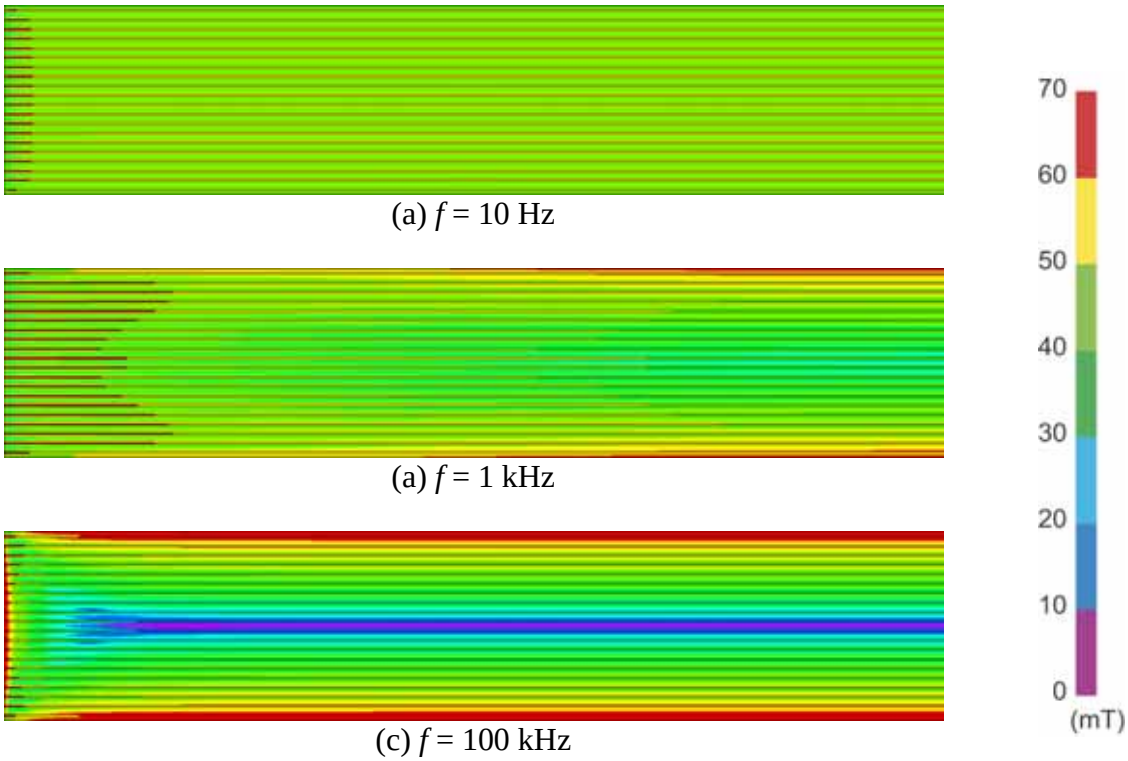

(a) f = 10 Hz

(a) f = 1 kHz

(c) f = 100 kHz

Fig. 3.4 Magnetic flux contours of multifilamentary YBCO coated conductor exposed to transverse magnetic field, where $\mu_0 H_m$ = 50 mT, ωt = 90 degrees, L = 100 mm, R_g = 1 μΩ, n_f = 20, w_f = 400 μm and w_g = 100 μm. Half of 100 mm-long conductor is shown (right side in figures is conductor center).

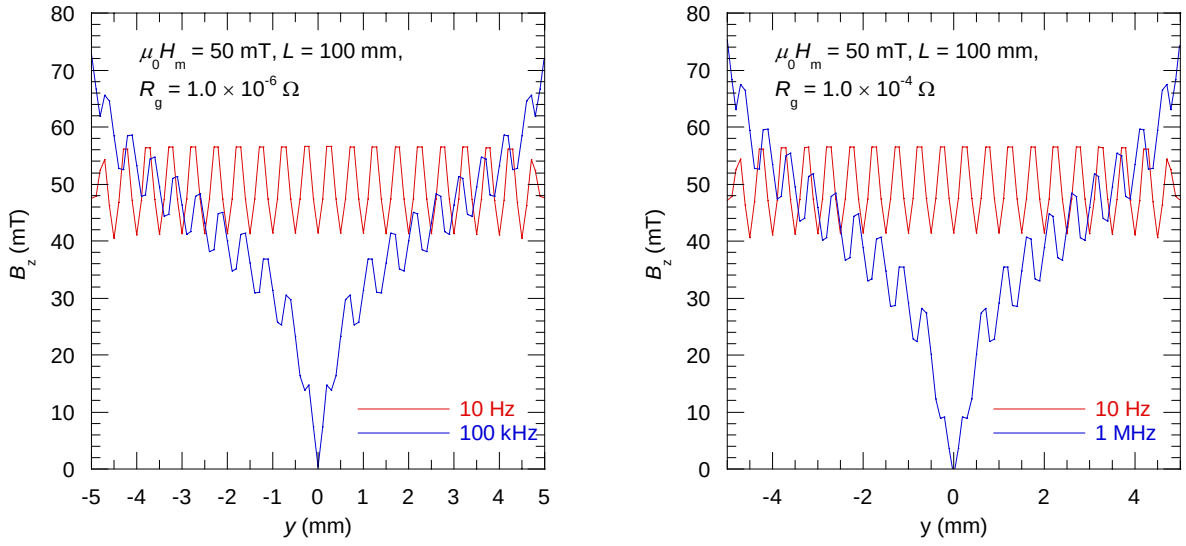

(a) R_g = 1 μΩ

(b) R_g = 100 μΩ

Fig. 3.5 Magnetic flux density profiles across multifilamentary YBCO coated conductors exposed to transverse magnetic field, where $\mu_0 H_m$ = 50 mT, ωt = 90 degrees, L = 100 mm, n_f = 20, w_f = 400 μm and w_g = 100 μm.

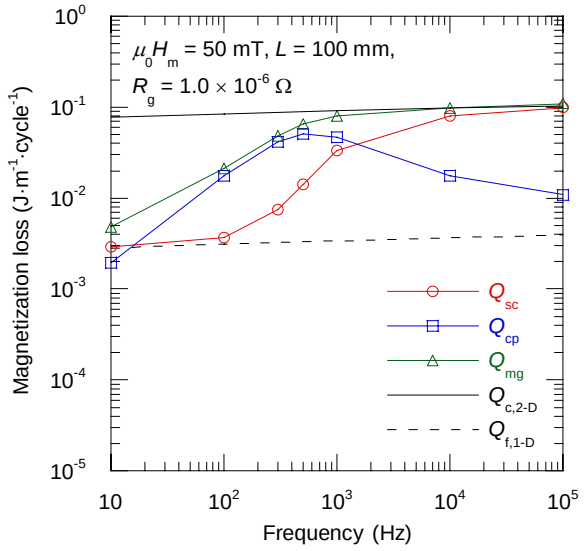

(a) Losses vs. frequency

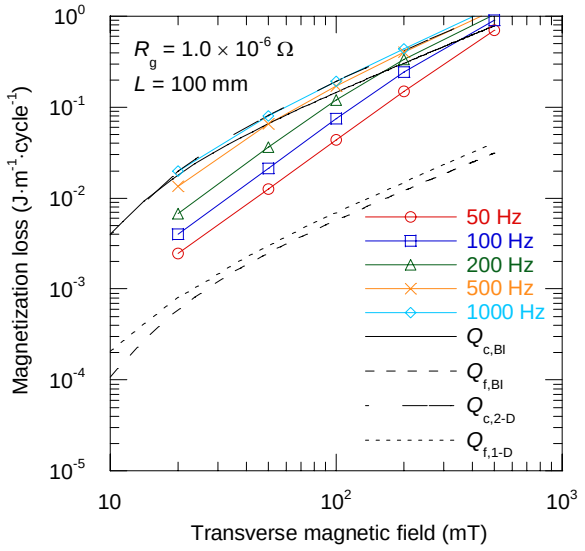

(b) Losses vs. field amplitude

Fig. 3.6 Overall magnetization loss and loss components of multifilamentary YBCO coated conductor where R_g = 1 μΩ.

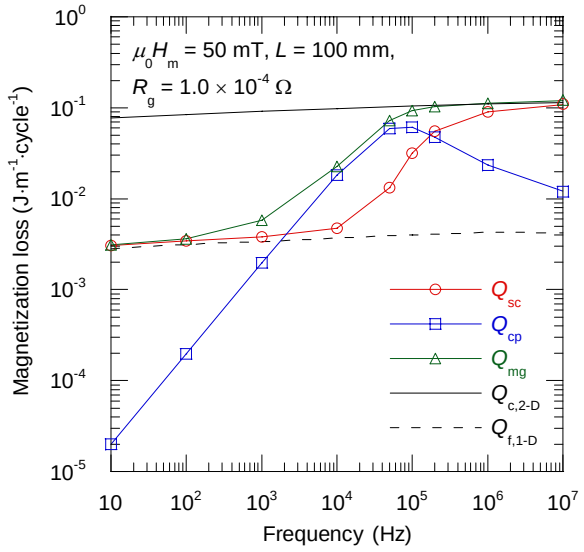

(a) Losses vs. frequency

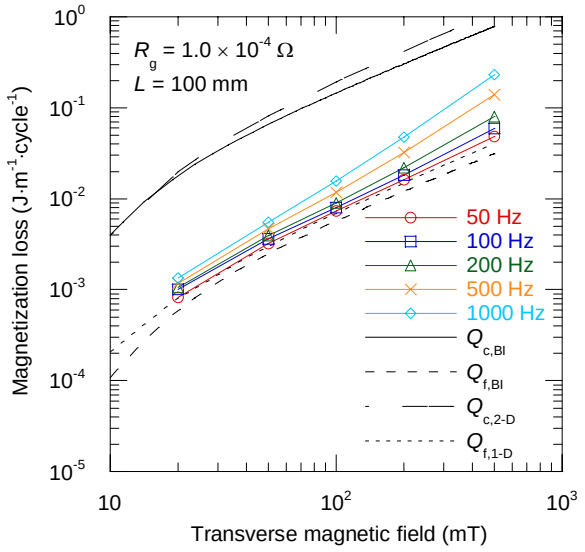

(b) Losses vs. field amplitude

Fig. 3.7 Overall magnetization loss and loss components of multifilamentary YBCO coated conductor where R_g = 100 μΩ.

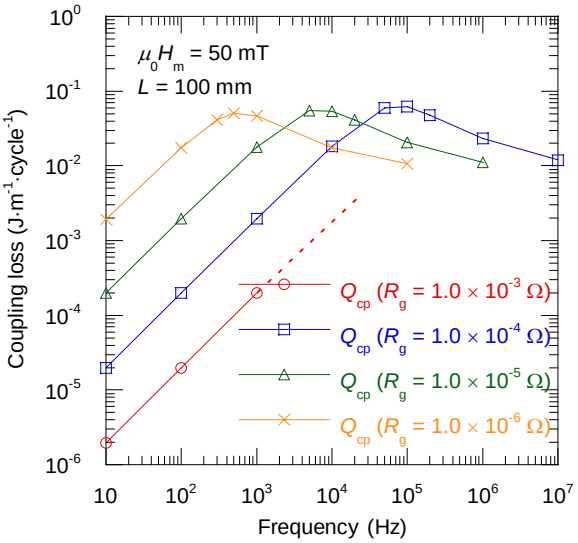

(a) Coupling loss vs. frequency

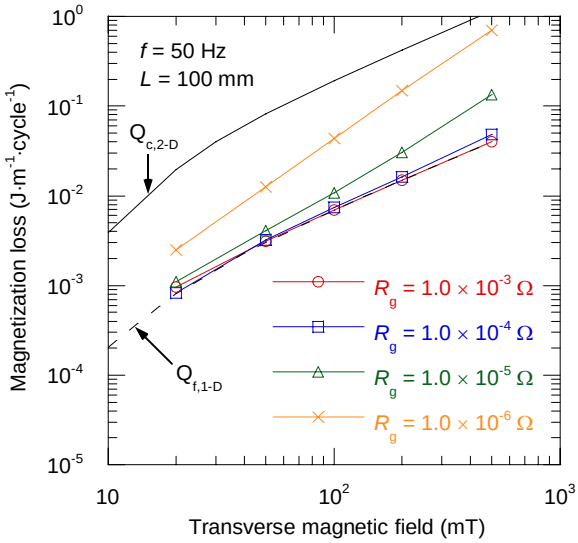

(b) Overall magnetization loss vs. field amplitude

Fig. 3.8 Influence of transverse resistance between filaments R_g on magnetization loss.

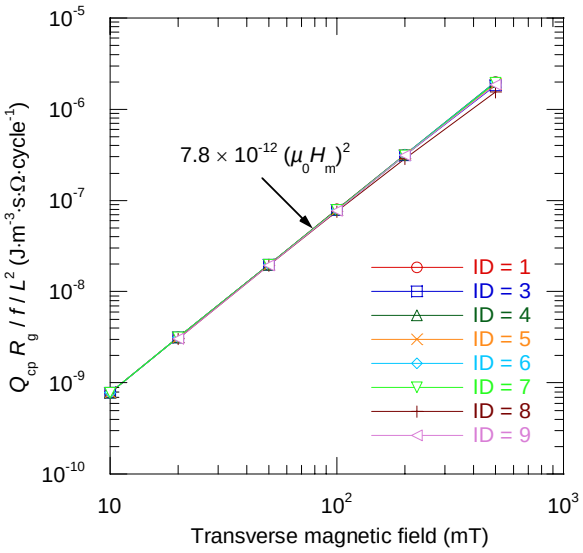

Fig. 3.9 Coupling loss Q_{cp} divided by (fL^2/R_g).

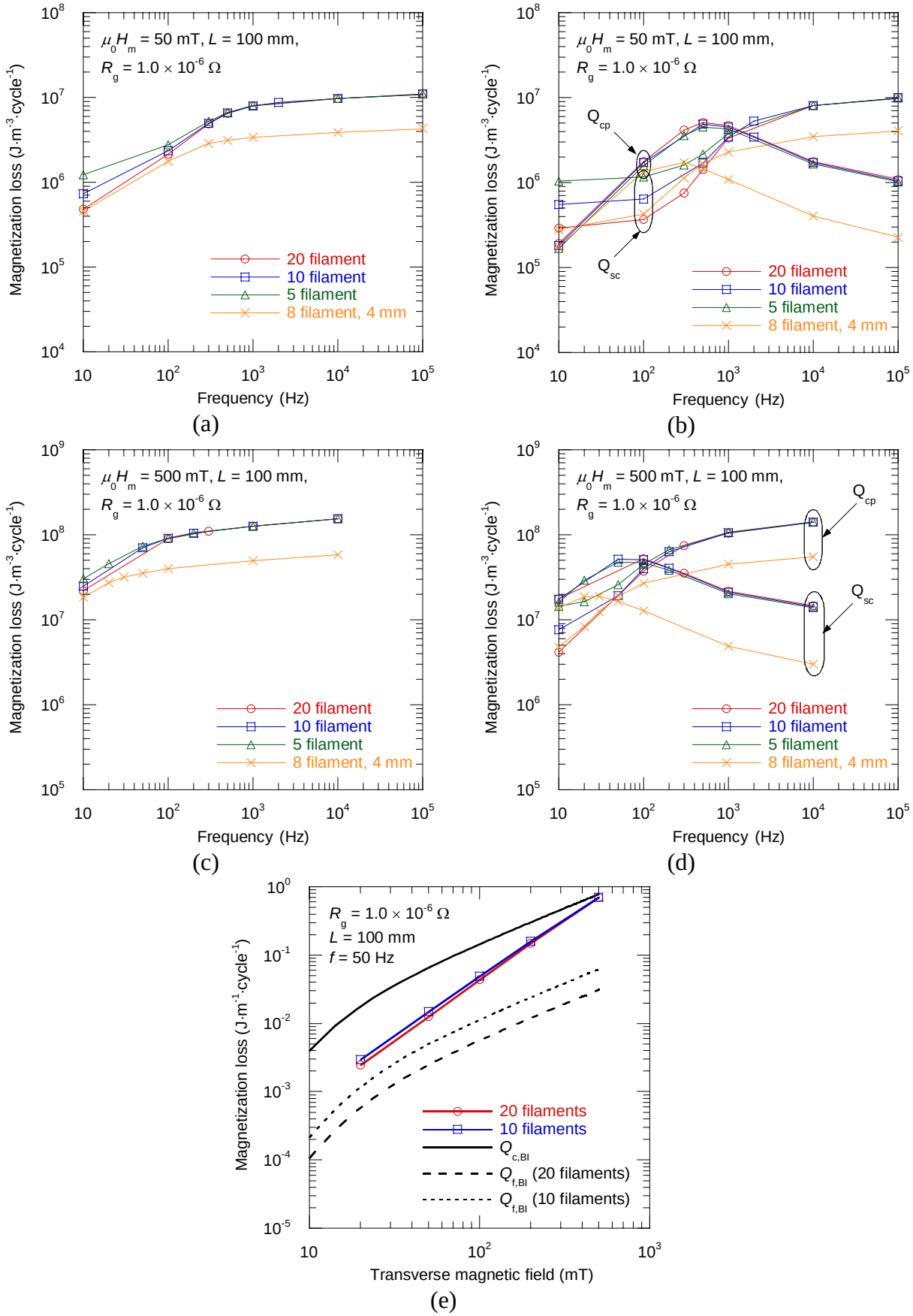

Fig. 3.10 Influence of number of filaments and width of conductor on magnetization loss where R_g = 1 μΩ.

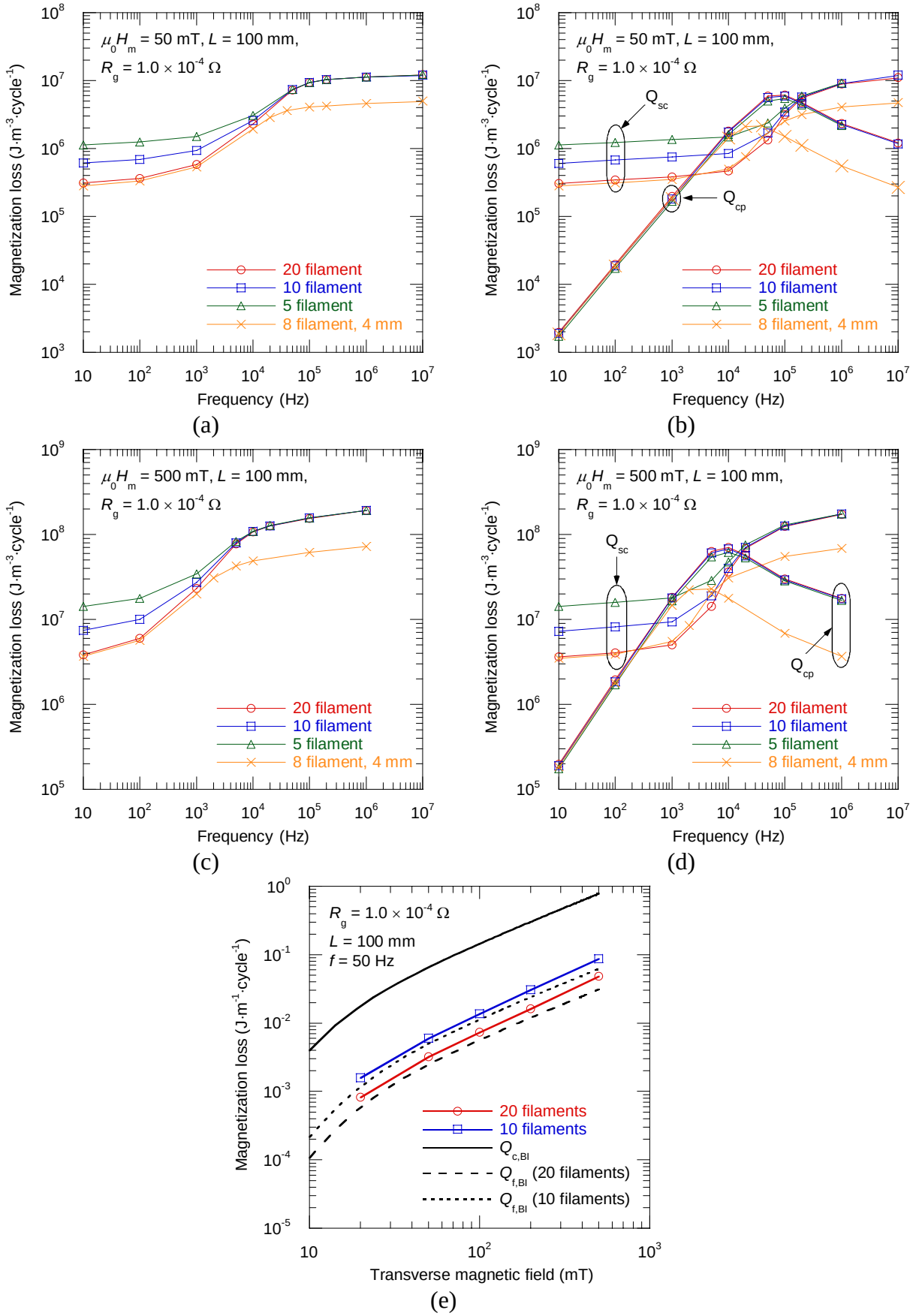

Fig. 3.11 Influence of number of filaments and width of conductor on magnetization loss where R_g = 100 μΩ.

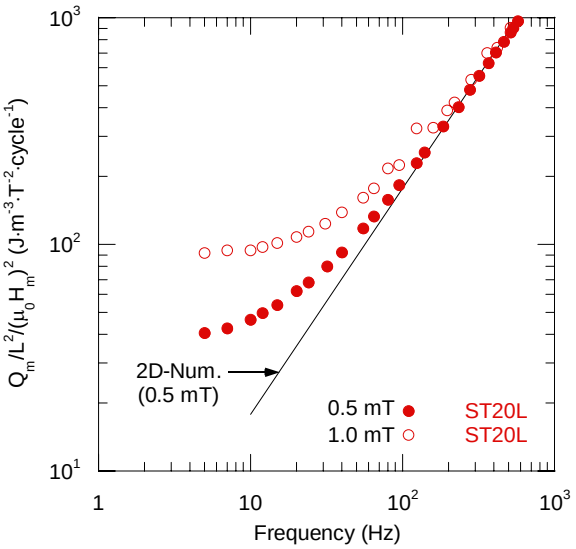

Fig. 3.12 Estimation of transverse resistance between filaments R_g of striated multifilamentary sample ST20 through comparison between measured loss and loss calculated by two-dimensional FEM model where L = 100 mm: calculated losses best fit to measured loss when R_g = 4 μΩ.

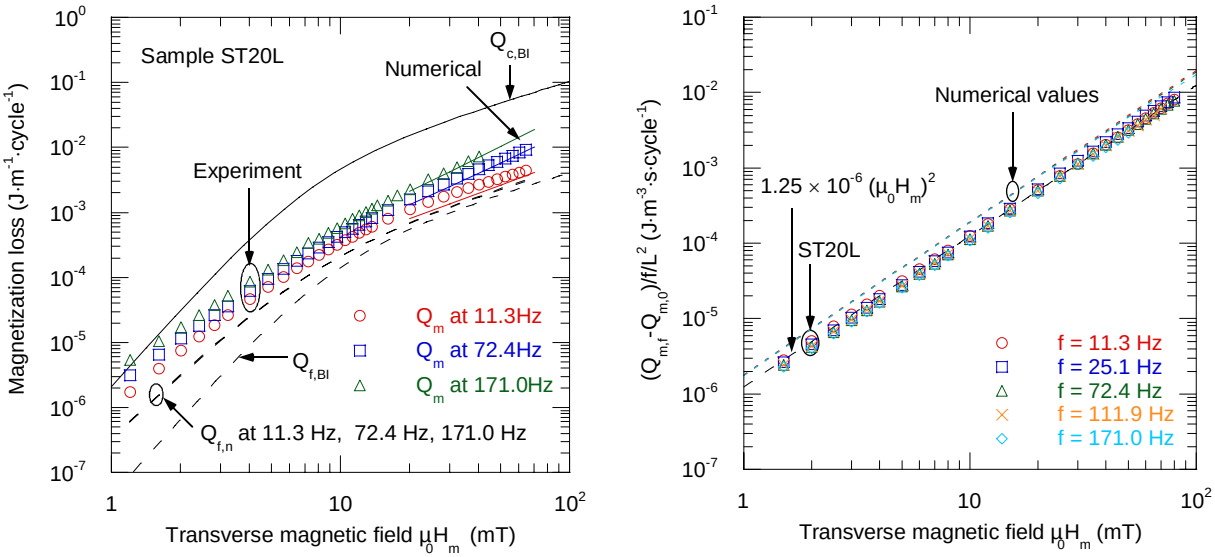

(a) Overall magnetization loss (b) Coupling loss component divided by fL^2

Fig. 3.13 Comparison between measured and calculated magnetization losses of striated multifilamentary sample ST20. R_g is set at 3 μΩ in calculations.

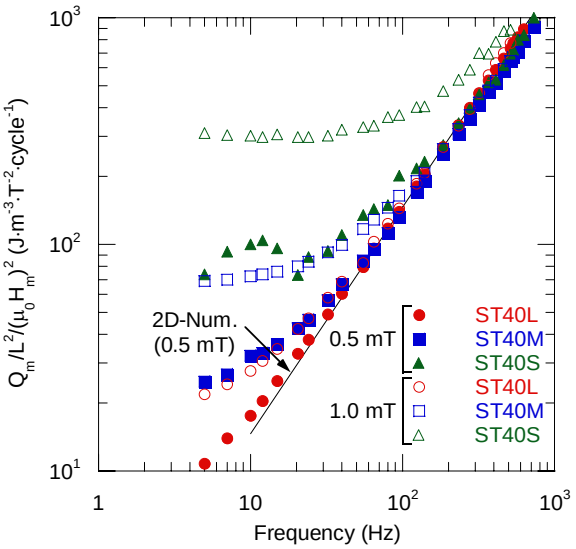

Fig. 3.14 Estimation of transverse resistance between filaments R_g of striated multifilamentary sample ST40 through comparison between measured loss and loss calculated by two-dimensional FEM model where L = 100 mm: calculated losses best fit to measured loss when R_g = 3 μΩ.

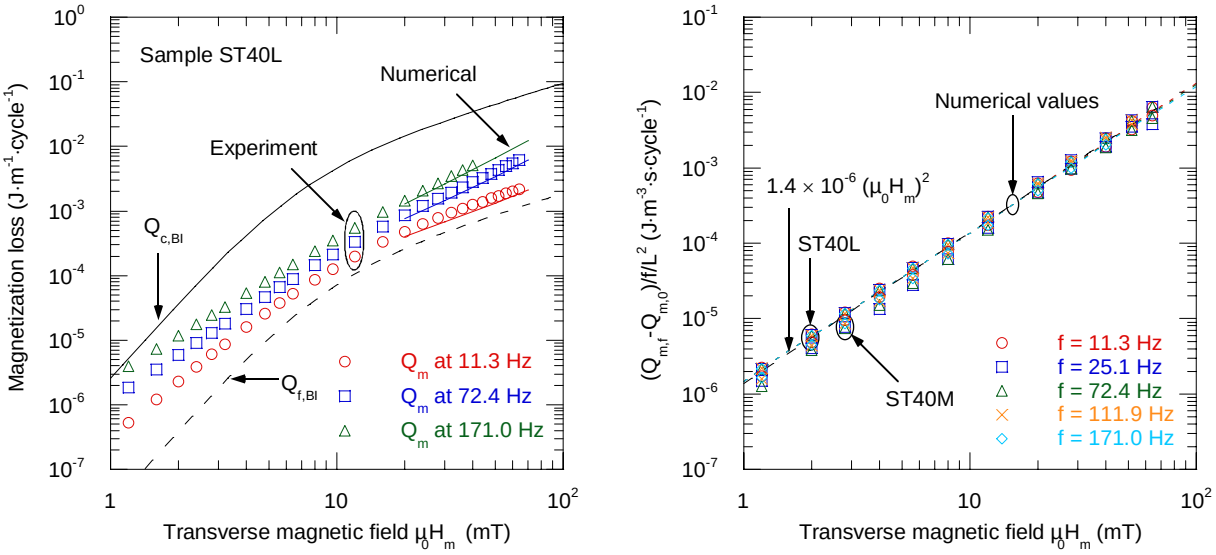

(a) Overall magnetization loss (b) Coupling loss component divided by fL^2

Fig. 3.15 Comparison between measured and calculated magnetization losses of striated multifilamentary sample ST40. R_g is set at 4 μΩ in calculations.

4. Summary

The reduction of the magnetization losses by the multifilamentary structure was demonstrated successfully. The measured magnetization losses of multifilamentary YBCO coated conductors apparently contain a hysteretic loss component in which the dissipated energy per cycle is independent of frequency and a coupling loss component in which the dissipated energy per cycle is proportional to frequency. Experimental results show that the striation for AC loss reduction is still effective even with the superconducting bridges between filaments.

Using the two-dimensional FEM model for electromagnetic field analysis of coated conductors, the AC losses at various conditions were calculated numerically. The calculated losses are typical frequency-dependent AC characteristics of multifilamentary superconductors. The transverse resistances between filaments in the measured samples were determined through the comparison between the measured and calculated magnetization losses at small field amplitude. The magnetization losses calculated in a wide range of field amplitude using these transverse resistances reasonably agree with the measured magnetization losses.

References

[1] Selvamanickam V, Lee H G, Li Y, Xiong X, Qiao Y, Reeves J, Xie Y, Knoll A and Lenseth K 2003 *Physica C* **392-396** 859-621

[2] Watanabe T, Shiohara Y and Izumi T 2003 *IEEE Trans. Appl. Supercond.* **13** 2445-5

[3] Usoskin A, Freyhardt H C, Issaev A, Dzick J, Knoke J, Oomen M P, Leghissa M and Neumueller H W 2003 *IEEE Trans. Appl. Supercond.* **13** 2452-7

[4] Rupich M W, Schoop U, Verebelyi D T, Thieme C, Zhang W, Li X, Kodenkandath T, Nguyen N, Siegal E, Buczek D, Lynch J, Jowett M, Thompson E, Wang J-S, Scudiere J, Malozemoff A P, Li Q, Annavarapu S, Cui S, Fritzemeier L, Aldrich B, Craven C, Niu F, Schwall R, Goyal A and Paranthaman M 2003 *IEEE Trans. Appl. Supercond.* **13** 2458-61

[5] Barnes P N, Rhoads G L, Tolliver J C, Sumption M D and Schmaeman K W 2005 *IEEE Trans. Magn.* **41** 268-73

[6] Ashworth S P, Maley M, Suenaga M, Foltyn S R and Willis J O 2000 *J. Appl. Phys.* **88** 2718-23

[7] Amemiya N, Jiang Z, Iijima Y, Kakimoto K and Saitoh T 2004 *Supercond. Sci. Technol.* **17** 983-8

[8] Amemiya N, Kasai S, Yoda K, Jiang Z, Levin G A, Barnes P N and Oberly C E 2004 *Supercond. Sci. Technol.* **17** 1464-71

[9] Amemiya N, Yoda K, Kasai S, Jiang Z, Levin G A, Barnes P N and Oberly C E 2005 *IEEE Trans. Appl. Supercond.* **15** 1637-42

[10] Cobb C B, Barnes P N, Haugan T J, Tolliver J, Lee E, Sumption M, Collings E and Oberly C E 2002 *Physica C* **382** 52-6

[11] Jiang Z and Amemiya N 2004 *Supercond. Sci. Technol.* **17** 371-9

[12] Brandt E H and Indenbom M 1993 *Phys. Rev. B* **48** 12893-906

[13] Ogawa J, Nakayama H, Odaka S and Tsukamoto O 2004 *Physica C* **412-414** 1021-5

[14] Mawatari Y 1996 *Phys. Rev. B* **54** 13215-21

[15] Mawatari Y 1997 *IEEE Trans. Appl. Supercond.* **7** 1216-9

[16] Kasai S and Amemiya N 2005 *IEEE Trans. Appl. Supercond.* **15** 2855-8

[17] Ichiki Y and Ohsaki H 2004 *Physica C* **412-414** 1015-20

[18] Sugita S and Ohsaki H 2002 *Physica C* **378-381** 1196-201

[19] Amemiya N, Murasawa S, Banno N and Miyamoto K 1998 *Physica C* **310** 16–29